Earth Surface Processes and Landforms
Earth Surf. Process. Landforms **33**, 962–984 (2008)
Published online in 15 January 2008 Wiley InterScience
(www.interscience.wiley.com) **DOI:** 10.1002/esp.1623

A Transport-Distance Approach to Scaling Erosion Rates: 2. Sensitivity and Evaluation of MAHLERAN

John Wainwright,[1]* Anthony J. Parsons,[1] Eva N. Müller,[2] Richard E. Brazier,[3] D. Mark Powell[4] and Bantigegne Fenti[5]

[1] *Sheffield Centre for International Drylands Research, Department of Geography, University of Sheffield, Sheffield, UK*
[2] *Institut für Geoökologie, Universität Potsdam, Potsdam, Germany*
[3] *Department of Geography, University of Exeter, Exeter, UK*
[4] *Department of Geography, University of Leicester, Leicester, UK*
[5] *Queensland Department of Natural Resources, Mines and Energy, Indooroopilly, Queensland, Australia*

**Correspondence to: John Wainwright, Sheffield Centre for International Drylands Research, Department of Geography, University of Sheffield, Winter Street, Sheffield S10 2TN, UK. E-mail: j.wainwright@sheffield.ac.uk*

Received 21 May 2007;
Revised 7 September 2007;
Accepted 27 September 2007

Abstract

In the first paper in this series, we demonstrated that most process-based erosion models have a series of in-built assumptions that led us to question their true process basis. An alternative soil-erosion model (MAHLERAN – Model for Assessing Hillslope-Landscape Erosion, Runoff And Nutrients) based upon particle-travel distance has been presented in the first paper in this series and this paper presents the first of two evaluations of the model. Here, a sensitivity analysis shows that the numerical model is consistent with the analytical model of Parsons *et al.* (2004) and demonstrates that downslope patterns of sediment flux on hillslopes are a complex interaction of rainfall intensity, duration and pattern; hillslope gradient; surface roughness and sediment size. This result indicates that the spatial scaling of sediment transfers on hillslopes is a non-trivial problem and will vary from point to point and from event to event and thus from year to year. The model is evaluated against field data from a rainfall-simulation experiment on an 18 m × 35 m plot for which there are sub-plot-scale data on runoff hydraulics and sediment flux. The results show that the model is capable of reproducing the sedigraph with an overall normalized root-mean-square error of 18·4% and Nash–Sutcliffe efficiency of 0·90. Spatial and temporal patterns of particle-size distributions of the eroded sediment are also reproduced very well, once erosion parameters have been optimized for the specific soil conditions.

Keywords: erosion; sediment transport; soil-erosion model; scaling; validation

Introduction

In a previous paper (Wainwright *et al.*, in press a), we demonstrated that current process-based models of soil erosion are flawed because of misconceptions about and misrepresentations of the process mechanisms involved. We developed an alternative model (MAHLERAN – Model for Assessing Hillslope-Landscape Erosion, Runoff And Nutrients), which we believe to be based upon a more robust conceptualization of soil-erosion processes. In this paper we evaluate this model. First, we employ a sensitivity analysis to demonstrate the general behaviour of the model under varying conditions, and to compare its output with the analytical results obtained by Parsons *et al.* (2004). As these analytical results have been demonstrated to be a good representation of observed patterns in the field across a range of scales (Parsons *et al.*, 2006), this approach provides a useful benchmark for model evaluation, especially in terms of processes.

Secondly, we compare the performance of MAHLERAN against field data obtained from a large rainfall-simulation experiment at Walnut Gulch Experimental Watershed, Arizona, USA. In order to carry out this comparison, it is necessary to discuss the model parameter requirements, which are in general sparse in comparison with other process-based erosion models. We also appraise the quality of measured field data, so that uncertainty can be incorporated in the model evaluation.

Model Sensitivity and Comparison to the Analytical Model of Parsons *et al.* (2004)

As a first stage of model evaluation, we undertake simulations using a DEM made up of a 100 m long × 30 m wide, uniform, planar slope. Infiltration rates were fixed at zero so that the hydrological behaviour of the model produced uniformly increasing runoff, with no complications from feedbacks due to runon infiltration. Baseline conditions were for a 30 min, 60 mm h^{-1} rainfall event on a 5° planar slope, with a uniform fine-grained sand particle size (model size class, $\varphi = 2$: see Table I for explanation of size classes) and a friction factor (*ff*) of 20. In this evaluation, we seek to determine the behaviour of response variables to changes in the input variables. Some instances show that monotonic changes in input variables yield monotonic changes in response variable. Others, on the other hand, do not demonstrate similar, monotonic responses, and we term these complex responses (as can be seen in appendix Figures A1–A4).

Sensitivity of the model was evaluated against changes in these conditions as shown in Table I. In the first set of sensitivity-analysis simulations, raindrop detachment is the sole mechanism for detachment as the effective concentrated-erosion detachment rate, $\delta_{\varepsilon,\varphi}$, is set to zero for comparison with the first case of Parsons *et al.* (2004), where only interrill erosion is considered. For the sake of brevity, the effects of the changes in conditions on the resulting downslope patterns of change in sediment flux, sediment yield and net erosion (Figure 1) are only summarized below. Full graphical output of these effects is given in the appendix Figures A1–A4.

Under all conditions the spatial pattern of sediment flux shows first an increase with distance downslope and then a decrease. The decrease becomes notably less marked beyond the peak as slope is increased or friction factor is reduced. In contrast, changing conditions of rainfall intensity and duration and particle size have less effect on the magnitude of the decrease. Lower rainfall intensities, greater rainfall durations, increasing slope gradients, greater presence of fine particles (either singly or in a mixed-size particle mix) and lower friction factors all cause the locus of maximum sediment flux to migrate downslope. The locus is closest to the top of the slope (at 4 m) when rainfall duration is set at 5 minutes and furthest downslope (at 73 m) for particle size-class 4 (in both cases with all other conditions set at baseline). The pattern of sediment yield is unaffected by changes in friction factor, is minimally affected by rainfall duration and is slightly affected by rainfall intensity. In contrast, changing conditions of particle size have a major impact on the pattern. For uniform particle sizes there is first an increase in sediment yield with distance downslope (with peak values at 2 m, 16 m and 59 m downslope for size-classes 2, 3 and 4, respectively), but there is no initial increase in the case of the mixed sediment. Net erosion changes from positive to negative in complex ways in response to changes in conditions. It is simplest for rainfall intensity and single particle sizes (occurring at decreasing distances downslope with increasing rainfall intensity, and decreasing particle sizes), but for rainfall duration it is more complicated, being >100 m for 5 min duration, 24 m for 10 min duration and returning to net erosion 39 m downslope, 22 m for 15 min duration and returning to net erosion 42 m downslope, and 21 m for 20 min duration, returning to net erosion >100 m downslope. In the case of slope angle, crossover of net erosion to net deposition occurs 20 m downslope at 5° and 26 m downslope at 10°. For the 15° slope, there is a minimum of net erosion at 36 m, before the rate again increases. For the mixed particle sizes there is a crossover from net erosion to net deposition at 18 m, but a return to net erosion at 82 m downslope. Changing friction factors also result in complex patterns of net erosion. There was no crossover between net erosion and deposition in the case of $ff = 2$, with simply a minimum value of net erosion 64 m downslope. For $ff = 20$, the crossover occurs at 22 m downslope, compared with 18 m for $ff = 40$ (returning to net erosion 96 m downslope) and 11 m downslope for $ff = 120$ (returning to net erosion 72 m downslope).

These sensitivity analyses all demonstrate the same downslope patterns of sediment flux and yield in unconcentrated overland flow as identified by the conceptual and analytical models of Parsons *et al.* (2004). Because of the differences in model structure, no one-to-one comparison can be made between the analytical and numerical versions, but they demonstrate the same behaviour, in particular near to the divide. The sensitivity analyses demonstrate that erosion fluxes and yields are likely to be highly dynamic near the top of the slope. This result has important implications for the design of plot-based experiments and the data produced from them, since plots are *de facto* mimicking conditions at the tops of slopes. Given that the fluxes and yields will be a complex function of storm variability, timing and intensity, surface conditions and dynamics (e.g. friction factors changing through the year due to vegetation growth and/or compaction following ploughing), it is important to recognize that the spatial patterns produced, and hence the ways in which data are subsequently scaled, will vary significantly. Crossover points from net erosion to net deposition also vary in a complex way including changes from conditions of net erosion to net deposition and in a number of cases back again, despite other factors being equal.

In a second set of sensitivity analyses concentrated erosion is active (setting $\delta_{\varepsilon,\varphi} = 152\ \mu m\ s^{-1}$), allowing the assessment of the relative importance of the different erosion mechanisms (Figure 2), again in relation to the conceptual model of Parsons *et al.* (2004). As for the first set of analyses, for the sake of brevity, the effects of the changes

DOI: 10.1002/esp

Table I. Summary of model sensitivity analysis comparing the effects of unconcentrated erosion only (by setting the effective concentrated-erosion detachment rate, $\delta_{\varepsilon_c,\varphi}$, to zero) with the case of mixed unconcentrated and concentrated erosion (using the baseline value of $\delta_{\varepsilon_c,\varphi} = 152$ μm s^{-1}). Baseline conditions (shown in italics for each parameter variation) represent a 30 min, 60 mm h^{-1} rainfall event on a 5° planar slope, with a uniform fine-grained sand particle size (model size class 2) and a friction factor of 20. Each parameter was varied (using the values given in the table) successively, keeping all others constant. More detail of individual simulations is provided in Figures 1, 2 and additional information Figures A1–A8

Parameter varied/value	Locus of maximum sediment flux (m)	Pattern of change of sediment yield	Crossover position from net erosion to net deposition (m)	Locus of maximum sediment flux (m)	Pattern of change of sediment yield	Crossover position from net erosion to net deposition (m)	Position of onset of concentrated erosion (m)	Percentage of raindrop detachment at base of slope (%)
Rainfall intensity	Unconcentrated erosion only ($\delta_{\varepsilon_c,\varphi} = 0$ μm s^{-1})			Unconcentrated and concentrated erosion ($\delta_{\varepsilon_c,\varphi} = 152$ μm s^{-1})				
20 mm h^{-1}	69	Peak <2 m from divide	>100	?	Peak <2 m from divide	None (minimum at 3 m)	92	77·2
40 mm h^{-1}	26	Peak <2 m from divide	46	50	Peak <2 m from divide	None (minimum at 45 m)	43	44·3
60 mm h^{-1}	*14*	*Peak <2 m from divide*	*21*	*36*	*Peak <2 m from divide*	*21 (net erosion from 31 m)*	*31*	*41·8*
80 mm h^{-1}	10	Exponential decrease	15	>100	Exponential decrease	15 (net erosion from 23 m)	23	41·0
Rainfall duration								
5 min	4	Peak <2 m from divide	>100	4	Peak <2 m from divide	None (minimum > 100 m)	n/a	100·0
10 min	7·5	Peak <2 m from divide	24 (net erosion from 39 m)	10	Peak <2 m from divide	24 (net erosion from 32 m)	32	57·6
15 min	10	Peak <2 m from divide	22 (net erosion from 42 m)	10	Peak <2 m from divide	22 (net erosion from 31 m)	31	52·8
30 min	*14*	*Peak <2 m from divide*	*21*	*36*	*Peak <2 m from divide*	*21 (net erosion from 31 m)*	*31*	*41·8*
Slope angle								
5°	*14*	*Peak <2 m from divide*	*21*	*36*	*Peak <2 m from divide*	*21 (net erosion from 31 m)*	*31*	*41·8*
10°	17	Exponential decline	26	>100	Exponential decline	26 (net erosion from 31 m)	31	47·9
15°	19·5	Exponential decline	none (minimum at 36 m)	>100	Exponential decline	None (minimum at 30 m)	31	52·2
Particle size*								
$\varphi = 2$	*73*	*Peak <2 m from divide*	*21*	*36*	*Peak <2 m from divide*	*21 (net erosion from 31 m)*	*31*	*41·8*
$\varphi = 3$	36	Peak at 16 m	68	69	Peak at 16 m	None (minimum at 1 m)	31	9·0
$\varphi = 4$	14	Peak at 59 m	>100	100	Peak at 59 m	None (minimum at 2 m)	31	51·8
φ = mixed**	12	Exponential decline	18 (net erosion from 82 m)	12	Exponential decline	18 (net erosion from 29 m)	31	83·2
Friction factor								
ff = 2	7	Peak between 2 & 3 m	none (minimum at 64 m)	>100·0	Peak between 2 & 3 m	21 (net erosion from 31 m)	31	53·6
ff = 20	*11*	*Peak <2 m from divide*	*21*	*11*	*Peak <2 m from divide*	*21 (net erosion from 31 m)*	*31*	*41·8*
ff = 40	14	Peak between 2 & 3 m	18 (net erosion from 96 m)	14	Peak between 2 & 3 m	18 (net erosion from 96 m)	n/a	100
ff = 120	35·5	Peak between 2 & 3 m	11 (net erosion from 72 m)	35·5	Peak between 2 & 3 m	11 (net erosion from 72 m)	n/a	100

* The current version of MAHLERAN uses the same six size classes as Wainwright *et al.* (1999a), namely $\varphi = 1$ (<63 μm), $\varphi = 2$ (63–125 μm), $\varphi = 3$ (125–1000 μm), $\varphi = 4$ (1–2 mm), $\varphi = 5$ (2–12 mm), $\varphi = 6$ (>12 mm).

** The 'mixed' particle-size case has the following percentages of each size class: 10·5% ($\varphi = 1$), 6·9% ($\varphi = 2$), 3·1% ($\varphi = 3$), 6·2% ($\varphi = 4$), 49·3% ($\varphi = 5$) and 24·0% ($\varphi = 6$), which is the same as for the subsequent model applications to the Walnut Gulch field site.

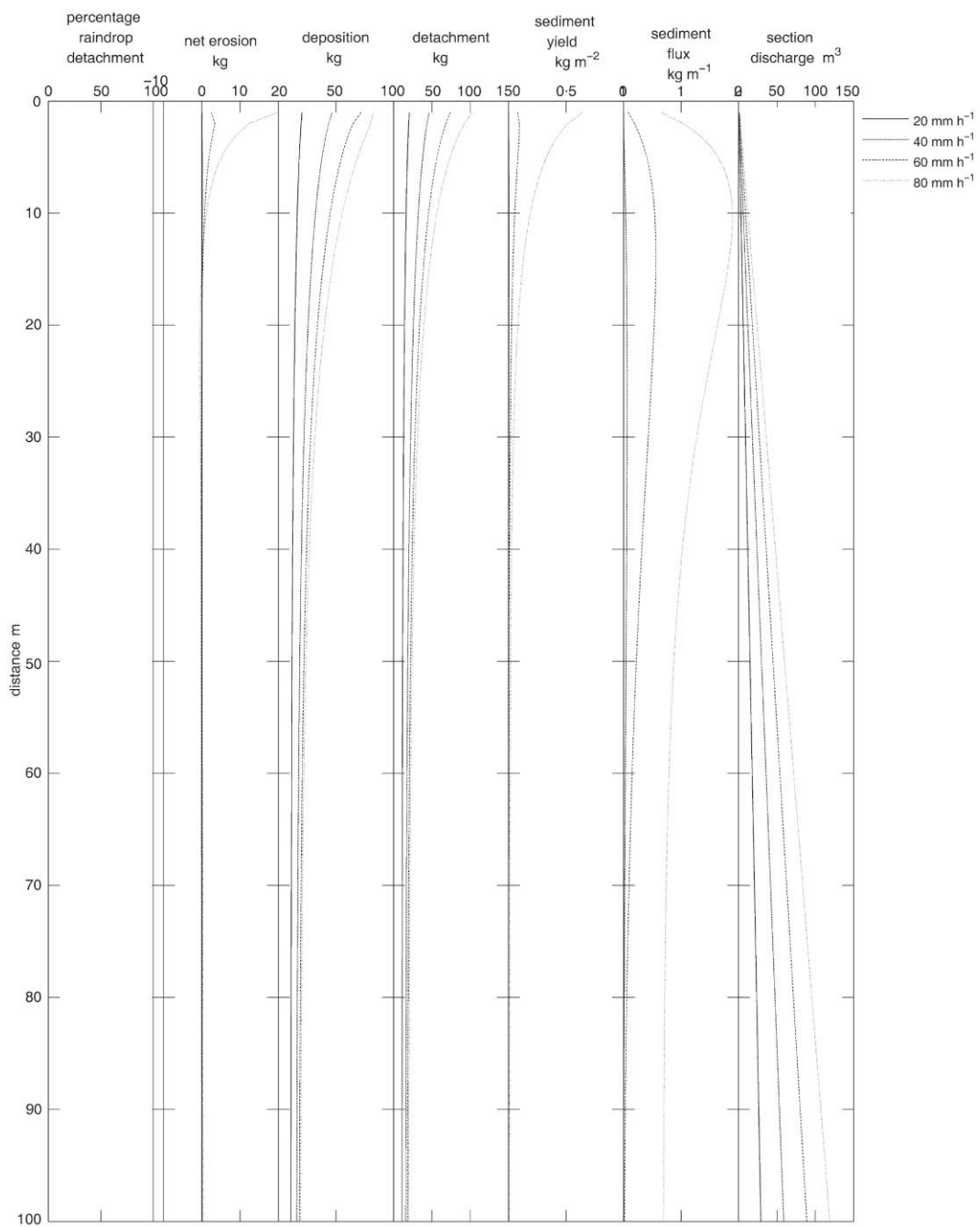

Figure 1. Sensitivity analysis on a uniform, planar 100 m long × 30 m wide slope according to rainfall intensity considering unconcentrated erosion only. The *x*-axis represents the distance from the top of the slope (0 m) to the base at 100 m. Each graph shows the sum of all the model cells at a given distance downslope for total flow discharge (m^3), sediment flux (kg m^{-1}), sediment yield (kg m^{-2}), detachment (kg), deposition (kg), net erosion (kg) and percentage of all detachment that is by raindrops (i.e. 100% = detachment entirely by raindrops, 0% = detachment entirely by concentrated flow erosion).

DOI: 10.1002/esp

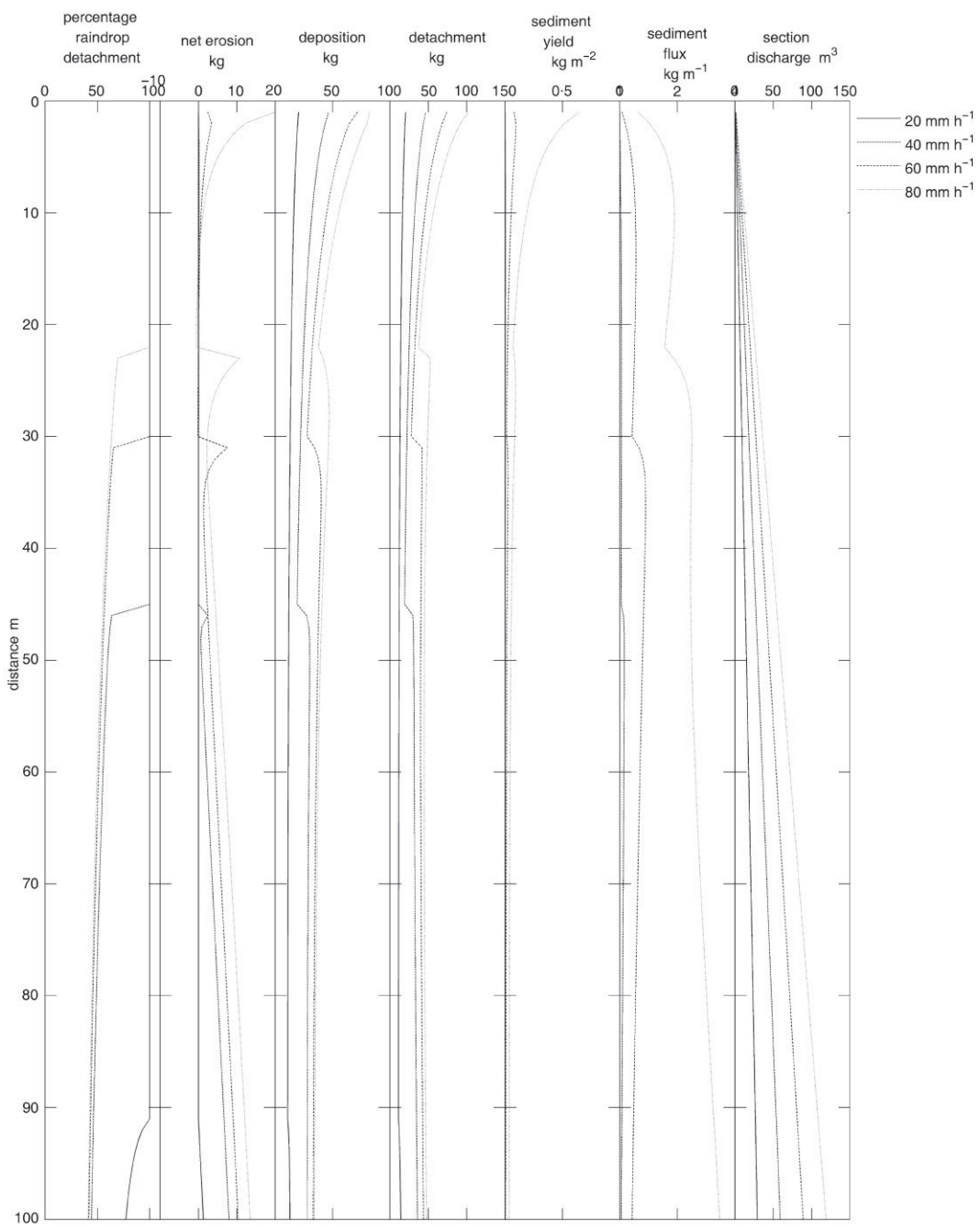

Figure 2. Sensitivity analysis on a uniform, planar 100 m long × 30 m wide slope according to rainfall intensity considering both unconcentrated and concentrated erosion.

in conditions on the resulting downslope pattern of change in sediment flux, sediment yield and net erosion is only summarised below, and full graphical output of these effects is given in appendix Figures A5–A8.

The location of the onset of concentrated erosion is not sensitive to slope gradient or particle size (Table I). The 5 minute duration event is too short to produce concentrated erosion, but for all longer events it commences at about the same distance downslope (c. 31 m). Only the lowest friction factor produces concentrated erosion, again at 31 m. In contrast, the threshold for concentrated erosion is strongly affected by rainfall intensity and moves progressively upslope with increasing rainfall intensity. Under conditions where concentrated erosion is initiated a secondary peak in sediment flux occurs, the location and magnitude of which varies with all changes to the base conditions. The relative importance of raindrop detachment (measured at the base of the 100 m slope) decreases with rainfall intensity and rainfall duration, but increases with gradient; there is a complex pattern in relation to particle-size variations.

The analytical model of Parsons *et al.* (2004) suggested that sediment flux should increase continuously under concentrated erosion where sediment supply is not limiting. The results of this set of sensitivity analyses show a number of cases where this pattern is reproduced, but a number of cases where it is not. Essentially, the difference is that the analytical model considers only concentrated erosion, whereas the numerical model considers the interaction of both concentrated and unconcentrated erosion. This interaction has been shown by Parsons and Wainwright (2006) to be a significant factor in the onset and permanence of rills on hillslopes. Wainwright *et al.* (2001) suggested that sediment yield should show a marked increase once the erosion domain passed from unconcentrated to concentrated erosion. The results of this sensitivity analysis again show that this suggestion is an oversimplification, and that the relative balance of the different erosion processes is the most critical control on the pattern observed.

Evaluation using Field Data

Model-evaluation data

To produce a rigorous test of the model in field conditions, data are required that can constrain all elements of the model, both temporally and spatially. As well as outflow hydrographs and sedigraphs, data are required on the spatial patterns of hydraulics and sediment flux. The results from a set of large rainfall-simulation experiments at Walnut Gulch Experimental Watershed, AZ, USA (31° 44′ 10″ N, 109°58′ 4″ W), published by Abrahams *et al.* (1991) and Parsons *et al.* (1990, 1991) provide possibly the only case where all these conditions are met. The runoff plot used in these experiments was 18 m wide and 35 m long, plan-planar, with slopes varying from 0° near the divide to 4·5° at the outlet, and located in a shrubland area, dominated by creosotebush (*Larrea tridentata*), albeit with a number of other shrub species including *Acacia constricta*, *Dasylirion wheeleri*, *Rhus microphylla* and *Yucca elata*, with a ground layer dominated by *Dyssodia acerosa* and *Zinnia pumila*. The soils on the hillslope on which the plot was situated are a gravelly loam developed on Quaternary alluvium (Gelderman, 1970), described as a loamy-skeletal, carbonatic, thermic, shallow Ustollic Palaeorthid (Breckenfield *et al.*, 1995). Calcareous accumulation horizons occur below the surface, and there is a well developed pavement surface, which has been shown to be the dominant control on infiltration rates (Abrahams *et al.*, 1989).

These experiments provide an almost unique dataset, in that, as well as having outflow (water and sediment) data, hydraulics and sediment data were collected during simulations along two transects S1 and S2, located 12·5 and 21 m from the upper plot boundary, respectively. Further details of the soil and vegetation conditions and experimental approach are given by Abrahams *et al.* (1991). In this paper, we have modelled the second experiment E2 carried out on this plot, in which 80 mm h^{-1} of rain was applied for a period of 20 min. The advantage of this example is that detailed assessments of the ability of MAHLERAN to reproduce the interrill hydrology and hydraulics of the event have already been carried out by Scoging *et al.* (1992) and Parsons *et al.* (1997), so we can be confident that there is a strong test of the erosion component of the model. As pointed out by Brazier *et al.* (2000), it is vitally important when evaluating process-based erosion models that are underpinned by hydrological and/or hydraulics models to evaluate the erosional response based on the best available hydrological modelling. It is particularly important to follow this approach when spatial data on erosion are required. In contrast with the published results of Abrahams *et al.* (1991), we have also considered how uncertainty in the field estimates of runoff and erosion might affect the model comparisons. Therefore, we have used the original data to calculate uncertainty estimates by deriving two estimates of the sediment yield at S1 and S2 and at the plot outlet. For S1 and S2, first we have followed the rating-equation method of Abrahams *et al.* (1991). Secondly, we have used sediment concentration in the samples taken at S1 and S2 together with the discharge estimates given by Parsons *et al.* (1990). Because the concentration data show a marked decline through the experiment, we have regressed sediment concentration against time and multiplied the discharge data by the estimate of sediment concentration given by this linear regression equation to obtain the second pair of values.

DOI: 10.1002/esp

For the plot outlet, we do not have data to employ the method of Abrahams *et al.* (1991). Instead we have similarly used the regression of sediment concentration against time and the discharge data of Parsons *et al.* (1990) as one method. Secondly, because at the outlet sediment concentration varied much less with time, we have simply multiplied the average sediment concentration by the discharge values. These different methods provide minimum and maximum estimates of fluxes at S1, S2 and the plot outlet and therefore describe the maximum range of uncertainty associated with observed fluxes.

Model parameterization

For application of the model to a specific site, spatial estimates of infiltration, flow roughness, vegetation and particle size characteristics are required. Infiltration parameterization requires spatially distributed estimates using the simplified Green and Ampt approach (Scoging *et al.*, 1992). The rainfall-simulation experiments of Parsons *et al.* (1996a) were carried out at the exact field site, allowing this approach to be parameterized directly. Final infiltration rate (K_s [mm min^{-1}]) is estimated using

$$K_s = 0{\cdot}351 + 0{\cdot}010\ rain - 0{\cdot}006\ P\%. \tag{1a}$$

where *rain* is the rainfall intensity [mm h^{-1}]
P% is the percentage of the ground surface covered by stone pavement [%].

The simplified Green and Ampt *b* parameter is distributed following the same experimental data as

$$b = 0{\cdot}785 + 0{\cdot}021\ P\% \tag{1b}$$

For the soils in question, a constant saturated soil-moisture content of 0·395 is used based on particle-size data following the method of Clapp and Hornberger (1978). The initial soil-moisture content was measured as 0·02, representing completely dry conditions.

The friction factor may be parameterized either using the simple depth feedback of Scoging *et al.* (1992),

$$ff = 14 - 0{\cdot}008\ h \tag{2}$$

where *h* is the depth of water flow [m],

or the more complex feedback based on flow and surface characteristics (Abrahams *et al.*, 1995), either in its original form,

$$ff = 1{\cdot}13 \times 10^{-6}\ \mathrm{Re}^{-0{\cdot}271}\ D_G^{1{\cdot}022}\ P\%^{3{\cdot}394} \tag{3a}$$

where Re is the flow Reynolds number [–]
D_{50} is the geometric mean grain size of the surface [mm],

or in the modified form,

$$ff = 9{\cdot}143 \times 10^{-6}\ \mathrm{Re}^{-0{\cdot}271}\ D_G^{1{\cdot}022}\ P\%^{3{\cdot}394} \tag{3b}$$

which accounts for the apparent underprediction of Equation (3a) compared with the data of Weltz *et al.* (1992 – see Parsons *et al.* (1994) and Wainwright *et al.* (2000) for a more detailed discussion). An alternative form is given by Abrahams *et al.* (1996), based on data from rill flows on hillslopes adjacent to the large shrubland plot, as follows:

$$ff = 1{\cdot}202\ Q^{-0{\cdot}317}\ D_G^{1{\cdot}383} \tag{3c}$$

where *Q* is the flow discharge [l s^{-1}].

A further feedback with strongly spatial characteristics is the relationship between rainfall kinetic energy and vegetation. As this relationship is highly dependent on specific vegetation characteristics (Brandt, 1989; Morgan, 1996), a function has been derived based on canopy cover of the same species as the dominant vegetation at the field sites:

DOI: 10.1002/esp

$$KE_v = KE(1 - 8{\cdot}1 \times 10^{-3}\ V\%) \quad (4)$$

where KE_v is the kinetic energy of rainfall arriving at the ground surface accounting for the effect of vegetation cover [J m^{-2} mm^{-1}]
$V\%$ is vegetation canopy cover [%].

This equation is based on experiments carried out by Wainwright *et al.* (1999b) on creosotebush (*Larrea tridentata*), which is the dominant shrub type on the rainfall-simulation plot (Abrahams *et al.*, 1991).

A digital elevation model (DEM) was obtained by surveying the plot on a 0·61 m grid. Surface conditions were characterized using quadrats on the same grid as the DEM to provide estimates of pavement and vegetation cover. Distributed particle-size information was then obtained using the information from the fine fractions as described by Parsons *et al.* (1991), scaled according to the percentage pavement cover.

Model evaluation

Equation (2) was used in the first instance to reproduce the results of Scoging *et al.* (1992) for the plot hydrology and hydraulics. The outflow hydrograph is reproduced with a Nash–Sutcliffe efficiency of 0·99 and normalized root-mean-square error (NRMSE) of 7·6%. At two cross-sections, 12·5 and 21 m from the divide, mean measured depths of flow across the 18 m plot width at steady state were 4·4 and 4·4 mm, respectively, compared with modelled depths of 4·4 and 5·1 mm, respectively. However, when zero depths are removed from the calculation, relating to the areas of the plot that were never inundated, the mean observed flow depth was actually 6·1 mm at the two cross sections. Thus, the modelled results, which are the means of the inundations of the individual cells, reflecting simulated inundation across the entire plot width, are a significant underestimate of the observed values. The mean measured velocities were 43·9 and 63·3 mm s^{-1}, compared with 28·0 and 35·9 mm s^{-1}, respectively. In other words, there is an issue relating to the mismatch of the point measurements in the field and the model, which represents conditions averaged over a cell (cf. also Tatard *et al.*, in press). Thus, within the constraints of spatial discretization of the model, both the overall hydrology and within-plot hydraulics of this event can be considered to be a good representation of overall flow depths and discharges, and a less good – but not unreasonable – representation of flow velocities. The implications of these differences will be considered in more detail below.

Figure 3 presents the outflow hydrograph and sedigraph for the event and comparative simulated data. The modelled sedigraph is an underestimate throughout the simulation, and it becomes progressively more so after the first four minutes. This difference produces an overall underestimate of 3·284 kg of total modelled sediment outflow compared with 19·272 kg observed (NRMSE = 96·4%, Nash–Sutcliffe = −1·75). At S1 and S2, the underestimates are comparable. Observed total sediment lies within the range of 3·650–7·703 kg at S1, compared with a modelled estimate of 1·286 kg; at S2, the observed range is 6·377–10·390 kg compared with the model estimate of 1·872 kg.

One reason for these differences may be the differences in the modelled flow hydraulics, in particular the underestimation of both flow depths and flow velocities, and corresponding overestimation of inundated width. Underestimating flow depth increases the rate of raindrop detachment (because of the protective effect of water flowing at the surface in Equation (9) in Wainwright *et al.*, in press a) but reduces flow detachment (via the link with shear velocity in Equation (10) in Wainwright *et al.*, in press a). Underestimates of depth and velocity also lead to underestimates of the transport distance in both unconcentrated and concentrated flows (via the feedback with flow energy in Equations (12) and (13), respectively, in Wainwright *et al.*, in press a), and of the virtual velocities of sediment particles (Equations (16) and (17) in Wainwright *et al.*, in press a). Thus, the pattern of hydraulics influences significantly the pattern of sediment entrainment and transport, and it does so in a potentially complicated way. Equations (3b) and (3c), which are thought to provide better representations of the flow–friction factor relationships as observed on small plots, were employed to evaluate whether any better representation of the hydraulics on the large plot could be obtained and what the consequence would be for modelled sediment patterns.

Equation (3b) produces an outflow hydrograph that is a slightly worse fit overall than Equation (2) (NRMSE = 10·7%, Nash–Sutcliffe = 0·98), and especially has problems fitting the initial part of the rising limb (Figure 3). The underestimation of the sedigraph is more extreme throughout. The total estimated sediment outflow is 2·672 kg (NRMSE = 100·7%, N–S = −1·99). These results arise despite a better representation of the mean flow depths (6·8 mm at S1 and 7·6 mm at S2 – albeit with the proviso noted above), due to the underestimation of flow velocities (17·8 and 39·5 mm s^{-1}, respectively) because of the overestimation of the inundated width. Although Equation (3c) is very similar to Equation (3b), it is based on experiments with higher flow rates, which are more realistic values for the large plot. The hydrograph is a better fit (NRMSE = 7·9%, N–S = 0·99) than with Equation (3b), although marginally worse than with Equation (2) (Figure 3). Total modelled plot sediment production was 4·202 kg, with a slightly better

DOI: 10.1002/esp

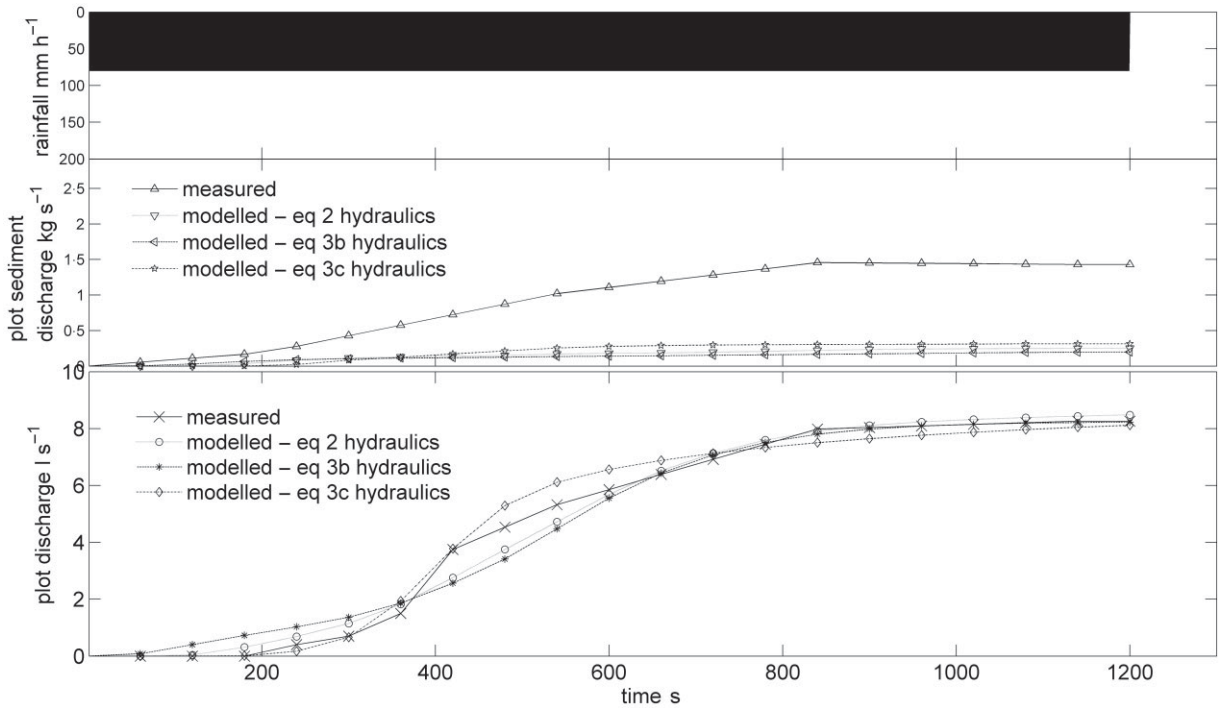

Figure 3. Observed and modelled plot hydrographs and sedigraphs for the E2 event on the large shrubland plot at Walnut Gulch, comparing the effects of using hydrology and hydraulics based on the approach of Scoging *et al.* (1992) – Equation (2) in the present paper – with those of Abrahams *et al.* (1995) – Equation (3b) in the present paper – and with those of Abrahams *et al.* (1996) – Equation (3c) in the present paper.

fit overall compared with Equation (2) (NRMSE = 90·0%, N–S = –1·40). However, the cross-sectional modelled sediment production is still significantly underestimated (1·900 and 2·957 kg, respectively), and the flow hydraulics are actually more poorly represented. Mean flow depths are significantly underestimated (1·6 and 1·8 mm, respectively) and mean flow velocities are significantly overestimated (70·3 and 94·2 mm s^{-1}, respectively). The better outflow fit is thus probably dominated by the response of the bottom part of the plot, which is dominated by rill-flow conditions akin to those employed in the derivation of Equation (3c).

An alternative explanation for the poor fit of the erosion estimates is that entrainment is inappropriately parameterized. In the case of raindrop detachment, the rates used in the above experiments were those derived by Wainwright *et al.* (1999a) for similar soils at Walnut Gulch, albeit in a different area and on lower angled slopes. Variation in these parameters and their conditions of measurement, coupled with a difficulty of parameterizing Equation (8) in Wainwright *et al.* (in press a) without detailed plot experiments, means that the parameters used will be subject to some uncertainty. The effect of this uncertainty can be evaluated most simply by carrying out a sensitivity analysis of the model to a_{φ} in Equation (8) in Wainwright *et al.* (in press a). There is also uncertainty in the estimate of concentrated flow detachment, because of the unknown effective detachment rate ($\delta_{\varepsilon_c,\varphi}$ in Equation (11) in Wainwright *et al.*, in press a). Various authors have considered this issue in the fluvial literature (as the effective detachment – or active layer – depth by ignoring the temporal scaling element), and estimates vary from using the D_{50} of the bed to more complex functions of bed porosity and relative grain size (Kelsey, 1996; Parker, 2007; the probabilistic approaches of Parker *et al.* (2000) simply serve to replace the active layer by two parameters). In the simulations above, $\delta_{\varepsilon_c,\varphi}$ equivalent to d_{50} per unit time was employed; a value of 152 μm s^{-1} was used, based on particle-size measurements reported by Parsons *et al.* (1991). Uncertainty in concentrated flow detachment can thus be evaluated by carrying out a sensitivity analysis to $\delta_{\varepsilon_c,\varphi}$.

For each of the three hydraulics conditions (Equations (2), (3b) and (3c)), the values of a_{φ} were varied using the Wainwright *et al.* (1999a) estimates for similar sites at Walnut Gulch as the base value, and using a multiplier of 0·01, 0·1, 0·5, 1 (base condition), 2, 3, 4, 5, 7·5 and 10 times, while $\delta_{\varepsilon_c,\varphi}$ was applied using values of 0 (no concentrated erosion), 76, 152 (base condition), 304, 608, 1216 and 2432 μm s^{-1}. A total of 210 simulations were thus carried out in this sensitivity analysis. Figure 4 shows the results of this analysis in terms of the effects on the estimated total

DOI: 10.1002/esp

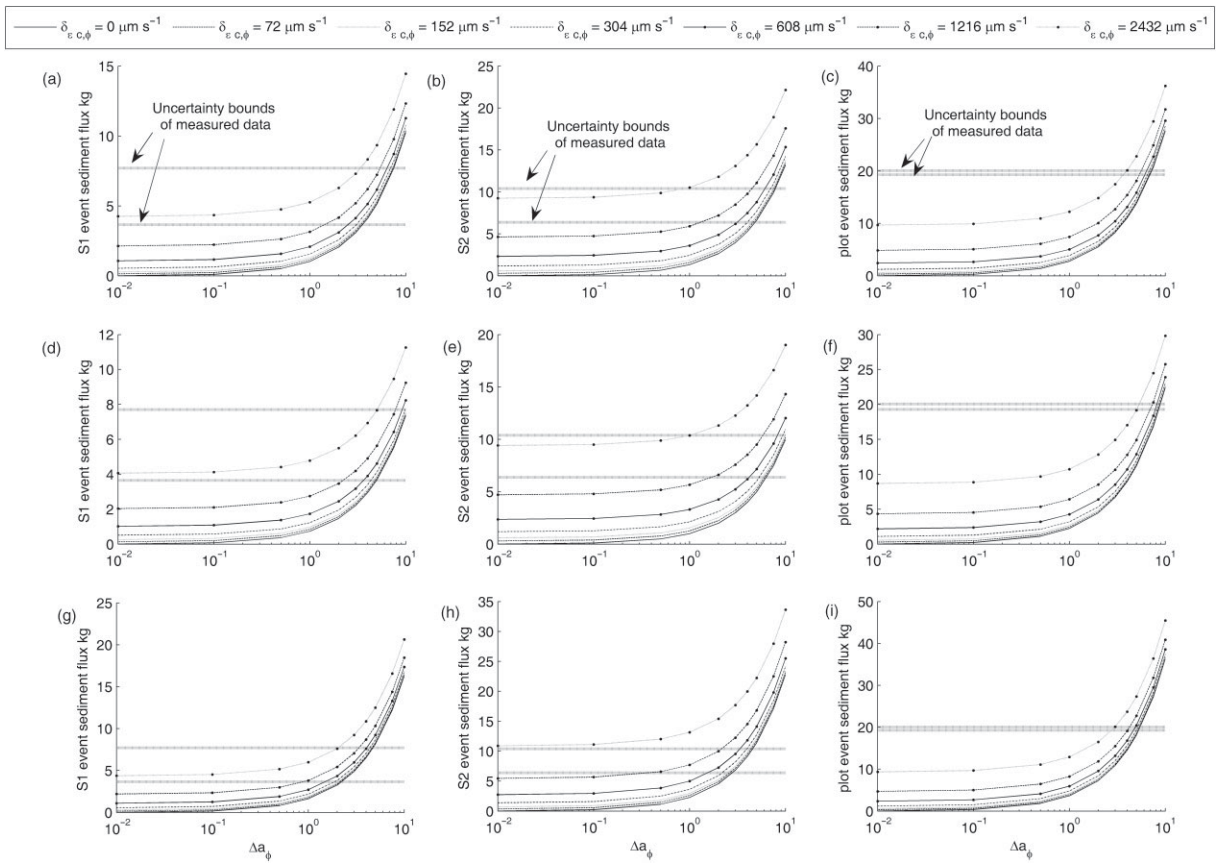

Figure 4. Results of sensitivity analysis of the response of sediment fluxes at the two within-plot cross sections (S1 located at 12·5 m from the upslope plot boundary, and S2 located at 21 m) and plot outlet on the shrubland large plot simulation to changes in a_ϕ (Δa_ϕ is the multiplier of the base values of a_ϕ) and $\delta_{\varepsilon_c,\varphi}$: (a)–(c) are results using Equation (2) hydraulics at S1, S2 and the outlet respectively; (d)–(f) are results using Equation (3b) hydraulics at S1, S2 and the outlet respectively and (g)–(i) are results using Equation (3c) hydraulics at S1, S2 and the outlet respectively. The heavy, dotted, horizontal lines show the lower and upper limits of the estimated observed values in all cases. Parameter combinations producing results within the bounds of these lines can be considered to replicate observed results, but note that acceptable parameter values must be constrained by the same combination of Δa_ϕ and $\delta_{\varepsilon_c,\varphi}$ for all three cases of S1, S2 and the plot outflow.

sediment fluxes at S1, S2 and the plot outlet and compares the results with the observed range of values at each point. It can be seen that the different hydraulic conditions provide different constraints on the combinations of values of a_φ and $\delta_{\varepsilon_c,\varphi}$ that are able to reproduce the observed erosion rates. Conditions are also less well constrained at the cross sections within the plots because of the higher uncertainties in the observed estimates of sediment flux. Although high values of $\delta_{\varepsilon_c,\varphi}$ can typically reproduce the observed estimates at the cross sections for a wide range of values of a_φ, it should be remembered that the implication of this combination of parameter values is that there is a significant amount of concentrated erosion taking place. Field observations of the location of rills and other concentrated flow paths would suggest that these parameter combinations are unrealistic (see Scoging *et al.*, 1992). In all cases, the flux is marginally more sensitive to relative changes in a_φ than relative changes in $\delta_{\varepsilon_c,\varphi}$, although there is a slight increase in sensitivity to relative changes in $\delta_{\varepsilon_c,\varphi}$ at S2 and the outflow, which would be expected given the more frequent occurrence of concentrated flows in these locations.

In terms of constraining the erosion rates by the observed data, acceptable values (within the margins of error on the observed data) are obtained with $\delta_{\varepsilon_c,\varphi} = 152\ \mu m\ s^{-1}$, the base value, and an a_φ multiplier of 7× when Equation (2) is used to estimate flow hydraulics or an a_φ multiplier of 8·75× when Equation (3b) is used to estimate flow hydraulics. It was not possible to constrain the parameters to fit all three points when Equation (3c) was used. It should be noted that these constraints are actually only a function of the relatively large margins of error in the estimates of sediment flux at the cross sections. An important implication of these results is that models that appear to be equifinal with

DOI: 10.1002/esp

respect to a range of parameter sets when evaluated against a single measuring point (usually the outflow) may not be (as) equifinal when evaluated against a much richer set of observations including multiple measuring points; further emphasizing the need for detailed spatial (and temporal) datasets for model evaluation.

The constrained parameters have then been used to simulate the sediment fluxes on the plot in detail. Figure 5 shows for the optimized sediment-transport parameters with Equation (2) hydraulics that the sedigraph tends to overestimate in the middle part of the event and underpredict from about minute 11, but has an overall acceptable fit (NRMSE = 18·4%, N–S = 0·90). In the equivalent case for the Equation (3b) hydraulics the pattern is similar but tends to be more extreme, producing a poorer fit (NRMSE = 28·6%, N–S = 0·76: Figure 5). Comparisons of the flow patterns (Figure 6) show that the discharge is spatially similar across the whole plot in both cases, yet the sediment transport at a point tends to be much more diffuse with the Equation (3b) case than the Equation (2) case. Although there are no direct measurements to evaluate which is the better representation of the actual experiment, comparison of the steady-state velocities shows much more concentration in the Equation (2) case than in the Equation (3b) case. These differences feed back to the erosion estimates via the stream-power terms in the transport-distance and virtual velocity calculations as noted above. The concentrated velocity field would seem the more acceptable based on dye-tracing observations during the event, further supporting the case that the sediment-transport rates optimized for Equation (2) hydraulics are the best estimates at present, despite the caveats relating to the understanding of the hydraulics across a complete range of values present at large plot or hillslope scales. Clearly, though, a detailed understanding of flow hydraulics is required because of the high sensitivity of the erosion model (and indeed others: see Wainwright and Parsons, 1998) to them.

Downslope patterns of estimated discharge and erosion characteristics are shown for both sets of conditions in Figure 7. Total discharge generally increases until about 29 m from the top of the plot, then decreases, as should be expected given the progressive narrowing of the plot to the outlet. Both hydraulic equations produce similar spatial patterns in this respect. Sediment flux increases steadily in both cases, albeit generally higher in the case of Equation (2), and increases relatively abruptly in the bottom 2–3 m of the plot, which is consistent with rill erosion in this location (Luk *et al.*, 1993), although the model only suggests a slight rise in concentrated versus unconcentrated

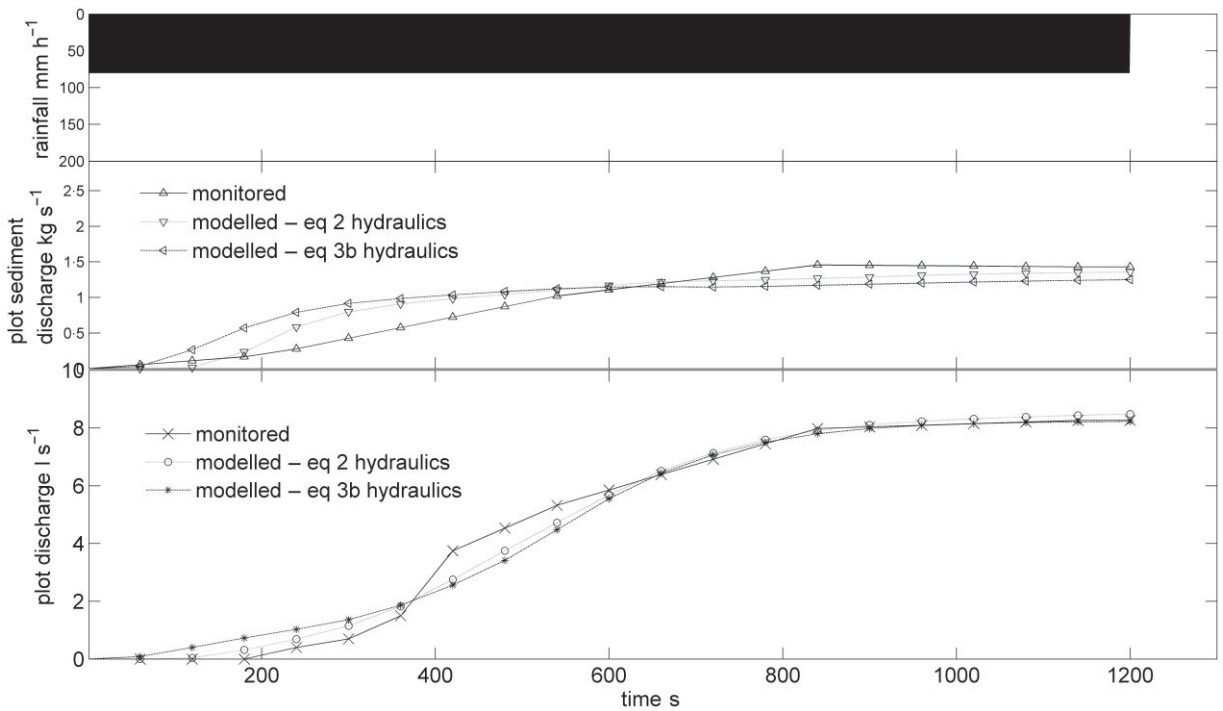

Figure 5. Observed and modelled plot hydrograph and sedigraph for the E2 event on the large shrubland plot at Walnut Gulch with sediment-transport parameters optimized for the field site using the sensitivity analysis discussed in the text, comparing the effects of using hydrology and hydraulics based on the approach of Scoging *et al.* (1992) – Equation (2) in the present paper – with those of Abrahams *et al.* (1995) – Equation (3b) in the present paper.

DOI: 10.1002/esp

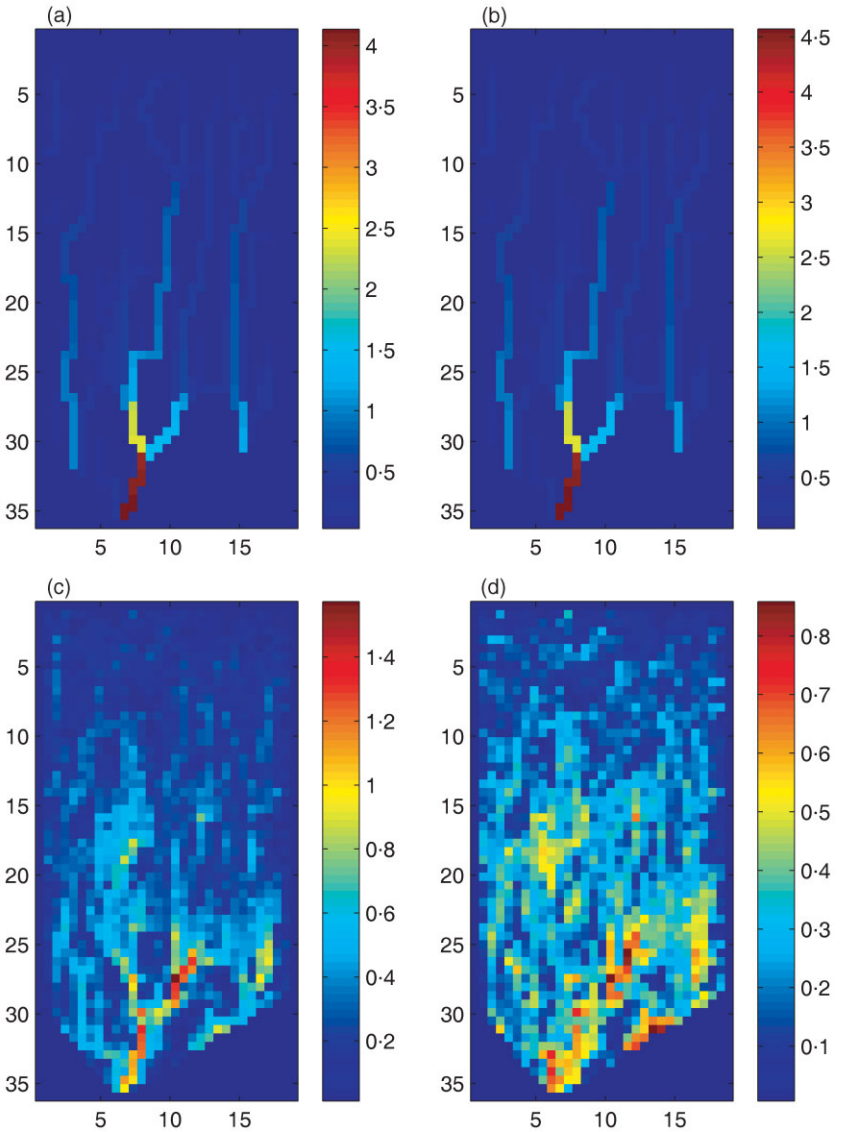

Figure 6. Comparisons of spatial patterns of runoff and sediment production for the E2 event on the large shrubland plot at Walnut Gulch: (a) total runoff in litres at a point for the Equation (2) case; (b) total runoff in litres at a point for the Equation (3b) case; (c) total sediment movement in kilograms at a point for the Equation (2) case; (d) total sediment movement in kilograms at a point for the Equation (3b) case. This figure is available in colour online at www.interscience.wiley.com/journal/espl

detachment at this location. However, sediment yield declines exponentially in a downslope direction, which is consistent with plot measurements (Parsons *et al.*, 1996b) and the conceptual basis of Parsons *et al.* (2004).

Particle-size data from the simulations are compared with the measured event data given by Parsons *et al.* (1991) in Table II. Overall, the model produces a close match to the observed percentages of silt plus clay and sand. However, within the event, there are some disparities, although these are limited to the period from 5 to 9 min. It should be noted that the observed eroded sediment includes some particles coarser than 2 mm (Parsons *et al.*, 1991, give the mean size of the coarsest 10 particles collected during minutes 15–19 as 3·7 mm), whereas the model produces an equivalent coarse fraction of 8×10^{-4}%, which is almost certainly an underestimate.

In summary, MAHLERAN seems able to reproduce the temporal and spatial dynamics of erosion on a large rainfall-simulation plot at Walnut Gulch. There is a need to account for the local characteristics of the soils at the site, which has been carried out through optimization due to the lack of any direct empirical data, and it is likely that this

DOI: 10.1002/esp

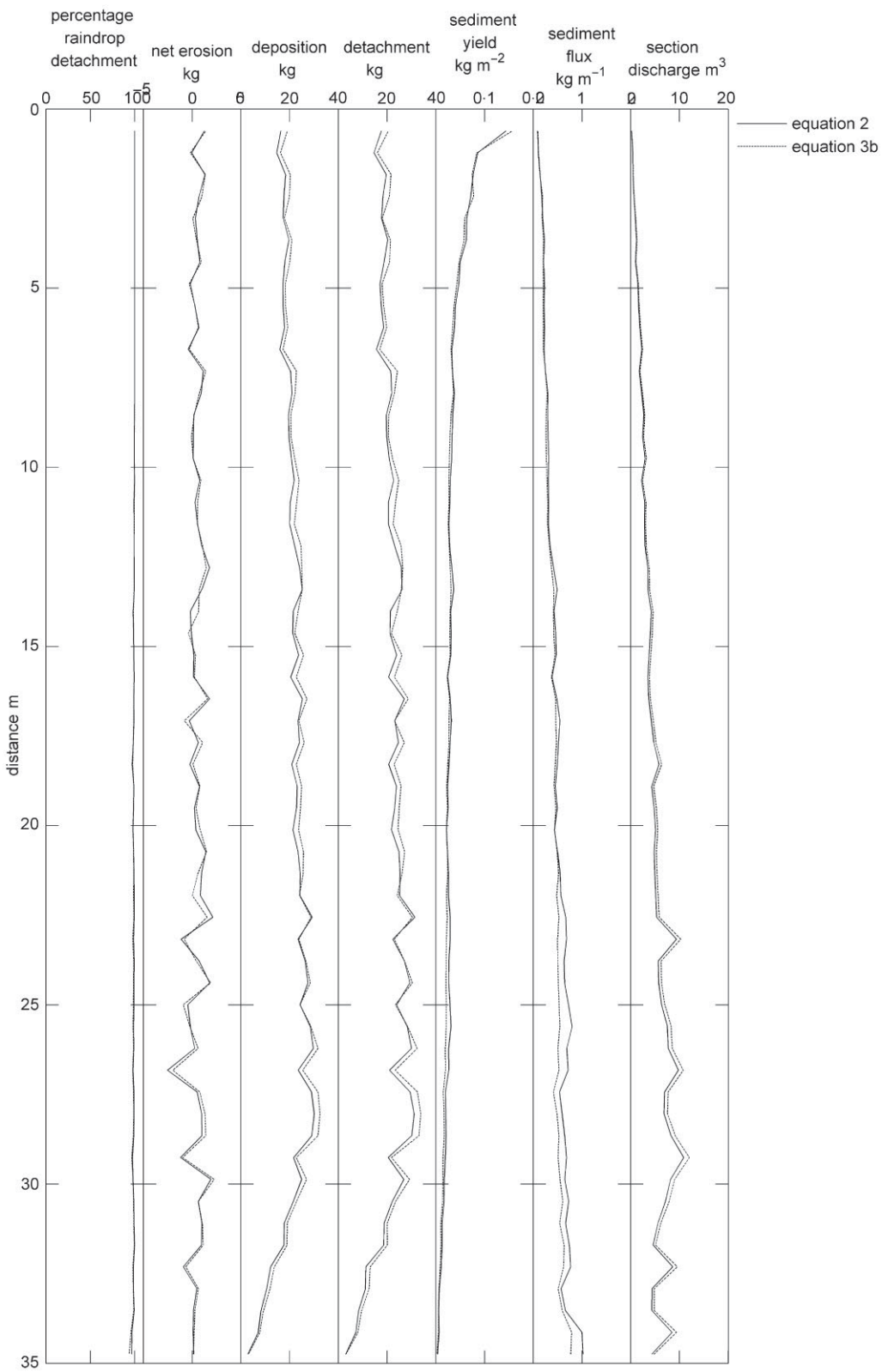

Figure 7. Summary of discharge and erosion characteristics of the simulations of E2 on the large shrubland plot at Walnut Gulch. The *x*-axis represents the distance from the top of the plot (0 m) to the outlet at 35 m.

Table II. Comparison of particle-size data from the rainfall-simulation plot at Walnut Gulch (from Parsons *et al.*, 1991) and the modelled simulations using Equation (2) and (3b) hydraulics

	Modelled silt & clay			Modelled sand		
Time (min)	Measured silt & clay	Equation (2)	Equation (3b)	Measured sand	Equation (2)	Equation (3b)
0–4	32%	35%	28%	68%	65%	72%
5–9	53%	30%	26%	47%	70%	74%
10–20	27%	31%	28%	73%	69%	72%

approach also ignores the dynamics of detachment and transport processes as noted above. The reproduction of particle-size characteristics for the start and end of the event is promising, but the poorer fit in the middle part of the event suggests that further work is required on such dynamics. The erosion dynamics are also a function of the representation of the hydraulics of the flow, and the two different approaches employed above suggest that there is an element of equifinality in the results according to the approximation used. For this reason, in the subsequent analyses (Wainwright *et al.*, in press b), both Equations (2) and (3b) have been employed to represent the flow hydraulics feedbacks, although it seems that Equation (2) is still the best available approximation given the current state of knowledge of the field site and the processes involved.

Conclusions

In this paper we have undertaken sensitivity analysis and testing of the soil-erosion model MAHLERAN first described and presented by Wainwright *et al.* (in press a). Sensitivity analysis of the model provides an indication of why it is difficult to scale erosion estimates spatially, in that the spatial variability of sediment fluxes will be a complex function of storm characteristics, slope form (both topographic and microtopographic) and soil composition. Verification of the model has been carried out by comparison with the analytical approach for unconcentrated flows as described by Parsons *et al.* (2004). There is no analytical approximation for mixed concentrated and unconcentrated flows, but for conditions where concentrated flows dominate the analytical approximation for concentrated conditions alone seems to hold.

Model evaluation has been carried out against detailed field measurements from a rainfall-simulation experiment for which the interrill hydrological characteristics have been well reproduced (Scoging *et al.*, 1992; Parsons *et al.*, 1997). These tests show that the detailed characteristics of flow hydraulics are critical in the ability of an erosion model to reproduce observed patterns of sediment flux, especially once the transition from unconcentrated to concentrated flow occurs. Furthermore, parameter optimization is required because of the constraints on existing information about the detachment and transport of sediment of different particle sizes, given the limitations from existing empirical data. However, once this optimization is carried out, it is possible to reproduce the spatio-temporal fluxes of sediment and its particle-size characteristics during the simulated event.

Acknowledgements

The field data were collected at Walnut Gulch Experimental Watershed over a period from 1988 to 1995. We are grateful to the respective research leaders at Southwest Watershed Research Center, Tucson, for their support, and the field staff at Walnut Gulch Experimental Watershed for their unstinting efforts. This work was funded by NERC grant GR3/12754 and NSF grant DEB 00-80412.

References

Abrahams AD, Li G, Parsons AJ. 1996. Rill hydraulics on a semiarid hillslope, southern Arizona. *Earth Surface Processes and Landforms* **21**: 35–47.

Abrahams AD, Parsons AJ, Luk S-H. 1989. Distribution of depth of overland-flow on desert hillslopes and its implications for modeling soil-erosion. *Journal of Hydrology* **106**: 177–184.

Abrahams AD, Parsons AJ, Luk S-H. 1991. The effect of spatial variability in overland-flow on the downslope pattern of soil loss on a semiarid hillslope, southern Arizona. *Catena* **18**: 255–270.

DOI: 10.1002/esp

Abrahams AD, Parsons AJ, Wainwright J. 1995. Controls and determination of resistance to overland flow on semiarid hillslopes, Walnut Gulch. *Journal of Soil and Water Conservation* **50**: 457–460.

Brandt CJ. 1989. The size distribution of throughfall drops under vegetation canopies. *Catena* **16**: 507–524.

Brazier RE, Beven KJ, Freer J, Rowan JS. 2000. Equifinality and uncertainty in physically based soil-erosion models: application of the GLUE methodology to WEPP – the Water Erosion Prediction Project for sites in the UK and US. *Earth Surface Processes and Landforms* **25**: 825–845.

Breckenfield DJ, Svetlik WA, McGuire CE. 1995. *Soil Survey of Walnut Gulch Experimental Watershed*. United States Department of Agriculture, Soil Conservation Service.

Clapp RB, Hornberger GM. 1978. Empirical equations for some soil–hydraulic properties. *Water Resources Research* **14**: 601–604.

Gelderman FW. 1970. *Soil Survey of Walnut Gulch Experimental Watershed: a Special Report*. US Department of Agriculture, Soil Conservation Service and Agricultural Research Service: Portland, OR.

Kelsey A. 1996. Modelling the sediment transport process. In *Advances in Fluvial Dynamics and Stratigraphy*, Carling PA, Dawson MR (eds). Wiley: Chichester; 229–261.

Morgan RPC. 1996. Verification of the European Soil Erosion Model (EUROSEM) for varying slope and vegetation conditions. In *Advances in Hillslope Processes*, Vol. 1, Anderson MG, Brooks SM (eds). Wiley: Chichester; 657–668.

Parker G. 2007. Transport of gravel and sediment mixtures. In *Sedimentation Engineering: Theories, Measurements, Modeling and Practice*, Garcia M (ed.). ASCE Manuals and Reports on Engineering Practice No. 110. Reston, VA.

Parker G, Paola C, Leclair S. 2000. Probabilistic Exner sediment continuity equation for mixtures with no active sediment layer. *Journal of Hydraulic Engineering* **126**: 818–826.

Parsons AJ, Abrahams AD, Luk S-H. 1990. Hydraulics of interrill overland-flow on a semiarid hillslope, southern Arizona. *Journal of Hydrology* **117**: 255–273.

Parsons AJ, Abrahams AD, Luk S-H. 1991. Size characteristics of sediment in interrill overland-flow on a semiarid hillslope, southern Arizona. *Earth Surface Processes and Landforms* **16**: 143–152.

Parsons AJ, Abrahams AD, Wainwright J. 1994. On determining resistance to interrill overland flow. *Water Resources Research* **30**: 3515–3521.

Parsons AJ, Abrahams AD, Wainwright J. 1996a. Responses of interrill runoff and erosion rates to vegetation change in Southern Arizona. *Geomorphology* **14**: 311–317.

Parsons AJ, Wainwright J. 2006. Depth distribution of interill overland flow and the formation of rills. *Hydrological Processes* **20**: 1511–1523.

Parsons AJ, Wainwright J, Abrahams AD. 1996b. Runoff and erosion on semi-arid hillslopes. In *Advances in Hillslope Processes*, Anderson MG, Brooks SM (eds). Wiley: Chichester; 1061–1078.

Parsons AJ, Wainwright J, Abrahams AD, Simanton JR. 1997. Distributed dynamic modelling of interrill overland flow. *Hydrological Processes* **11**: 1833–1859.

Parsons AJ, Wainwright J, Powell DM, Kaduk J, Brazier RE. 2004. A conceptual model for understanding and predicting erosion by water. *Earth Surface Processes and Landforms* **29**: 1293–1302.

Scoging HM, Parsons AJ, Abrahams AD. 1992. Application of a dynamic overland flow hydraulic model to a semi-arid hillslope, Walnut Gulch, Arizona. In *Overland Flow: Hydraulics and Erosion Mechanics*, Parsons AJ, Abrahams AD (eds). University College London Press: London; 105–145.

Tatard L, Planchon O, Nord G, Favis-Mortlock D, Wainwright J, Silvera N, Ribolzi O, Esteves M, Huang C-H. In press. 'Measurement and Modelling of high-resolution flow-velocity data under simulated rainfall on a low-slope sandy soil'. *Journal of Hydrology*. DOI: 10.1016/j.hydrol.2007.07.016

Wainwright J, Parsons AJ. 1998. Sensitivity of sediment-transport equations to errors in hydraulic models of overland flow. In *Modelling Soil Erosion by Water*, Boardman J, Favis-Mortlock D (eds). Springer: Berlin; 271–284.

Wainwright J, Parsons AJ, Abrahams AD. 1999a. Field and computer simulation experiments on the formation of desert pavement. *Earth Surface Processes and Landforms* **24**: 1025–1037.

Wainwright J, Parsons AJ, Abrahams AD. 1999b. Rainfall energy under creosotebush. *Journal of Arid Environments* **43**: 111–120.

Wainwright J, Parsons AJ, Abrahams AD. 2000. Plot-scale studies of vegetation, overland flow and erosion interactions: case studies from Arizona and New Mexico. *Hydrological Processes* **14**: 2921–2943.

Wainwright J, Parsons AJ, Müller EN, Brazier RE, Powell DM, Fenti B. In press a. A transport-distance approach to scaling erosion rates: 1. Background and model development. *Earth Surface Processes and Landforms*. DOI: 10.1002/esp1624

Wainwright J, Parsons AJ, Müller EN, Brazier RE, Powell DM, Fenti B. In press b. A transport-distance approach to scale erosion rates: 3. Evaluating Scaling Characteristics of Mahleran. *Earth Surface Processes and Landforms*. DOI: 10.1002/esp1622

Wainwright J, Parsons AJ, Powell DM, Brazier RE. 2001. A new conceptual framework for understanding and predicting erosion by water from hillslopes and catchments. In *Soil Erosion Research for the 21st Century. Proceedings of the International Symposium*, Ascough JC II, Flanagan DC (eds). American Society of Agricultural Engineers: St Joseph, MI; 607–610.

Weltz MA, Arslan AB, Lane LJ. 1992. Hydraulic roughness coefficients for native rangelands. *Journal of Irrigation and Drainage Engineering – ASCE* **118**: 776–790.

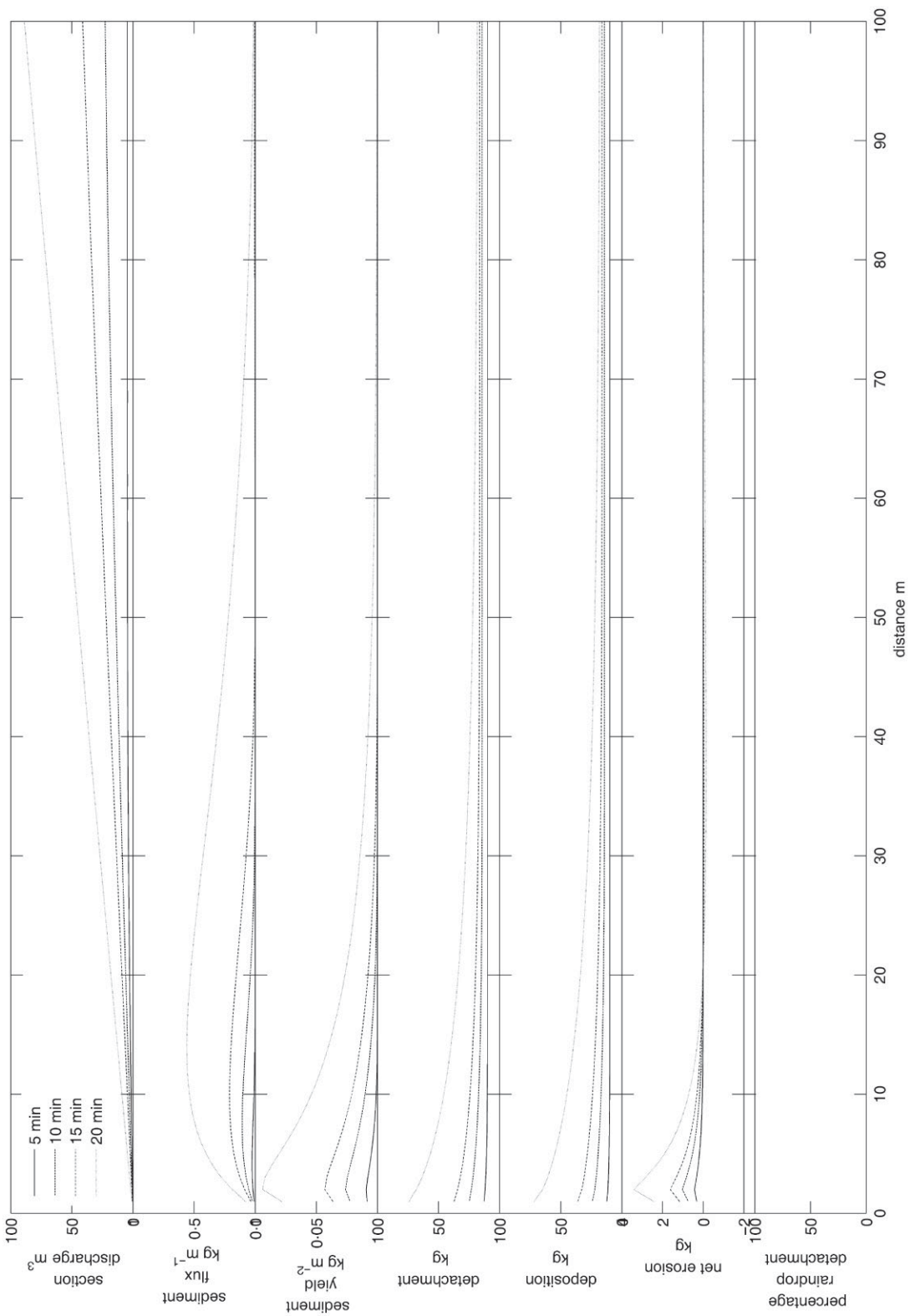

Figure A1. Sensitivity analysis on a uniform, planar 100 m long × 30 m wide slope according to rainfall duration considering unconcentrated erosion only. The *x*-axis represents the distance from the top of the plot (0 m) to the outlet at 35 m. Each graph shows the sum of all the model cells at a given distance downslope for total flow discharge (m^3), sediment flux (kg m^{-1}), sediment yield (kg m^{-2}), detachment (kg), deposition (kg), net erosion (kg) and percentage of all detachment that is by raindrops (i.e. 100% = detachment entirely by raindrops, 0% = detachment entirely by concentrated flow erosion).

DOI: 10.1002/esp

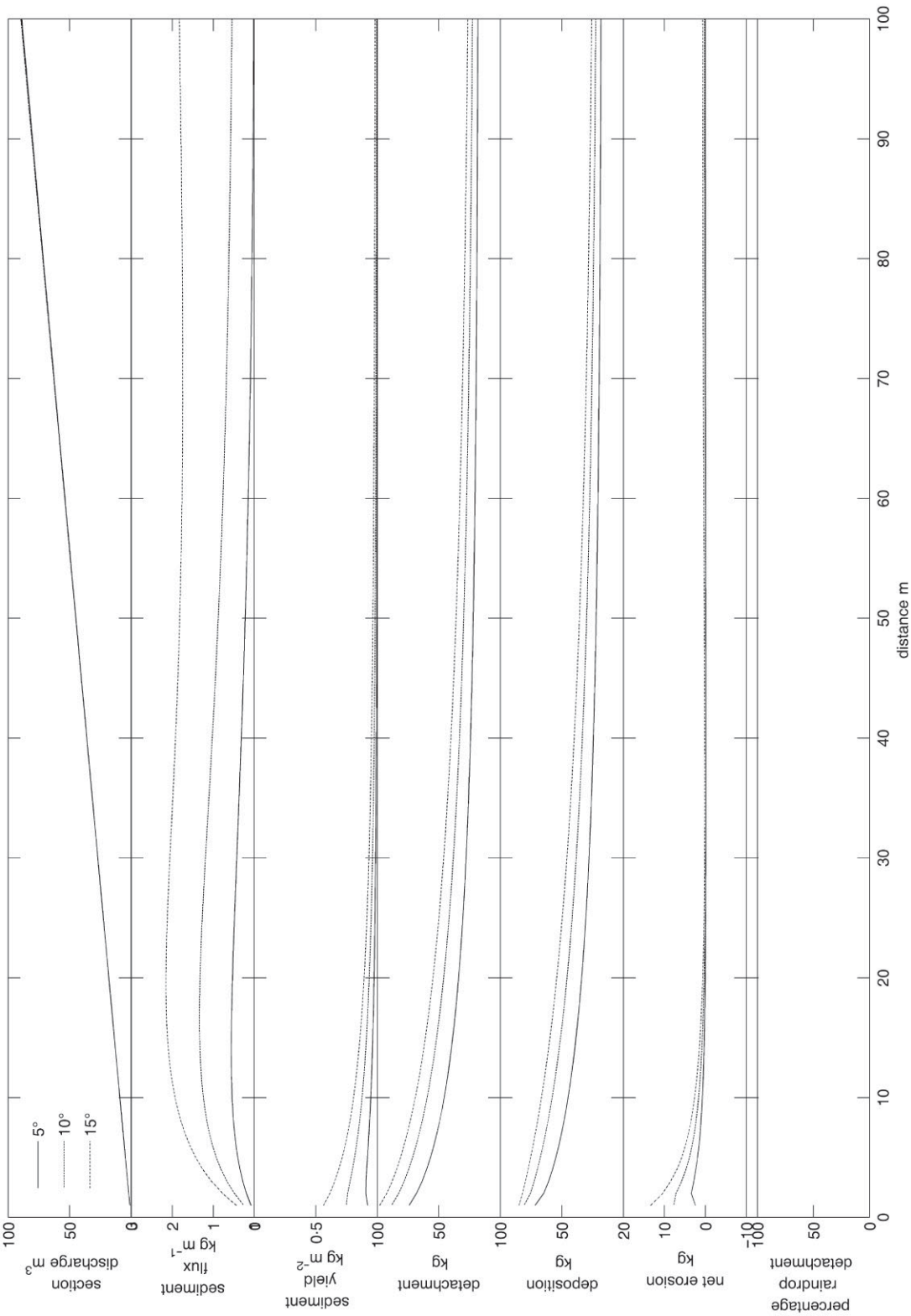

Figure A2. Sensitivity analysis on a uniform, planar 100 m long × 30 m wide slope according to slope angle considering unconcentrated erosion only.

DOI: 10.1002/esp

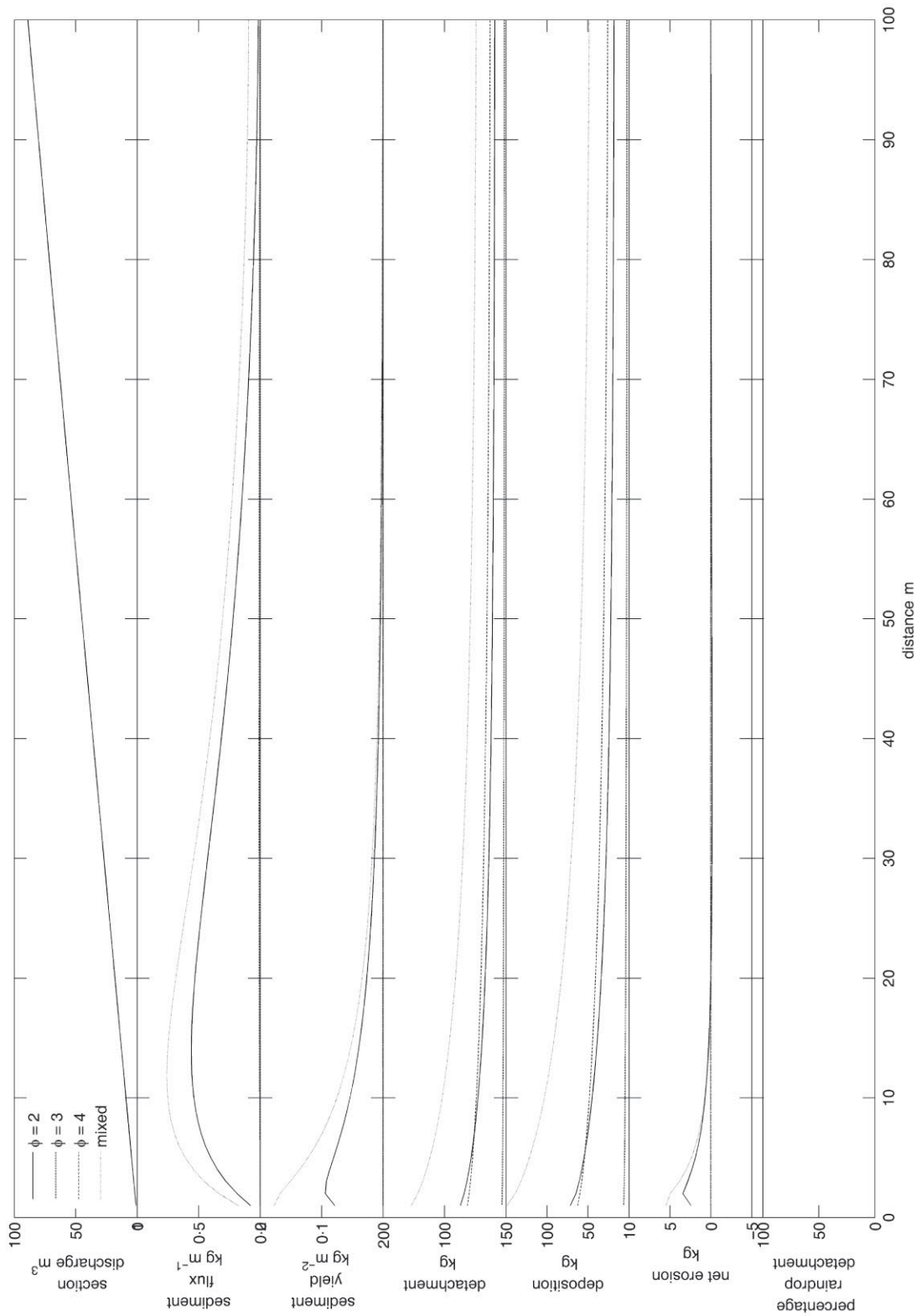

Figure A3. Sensitivity analysis on a uniform, planar 100 m long × 30 m wide slope according to grain size considering unconcentrated erosion only.

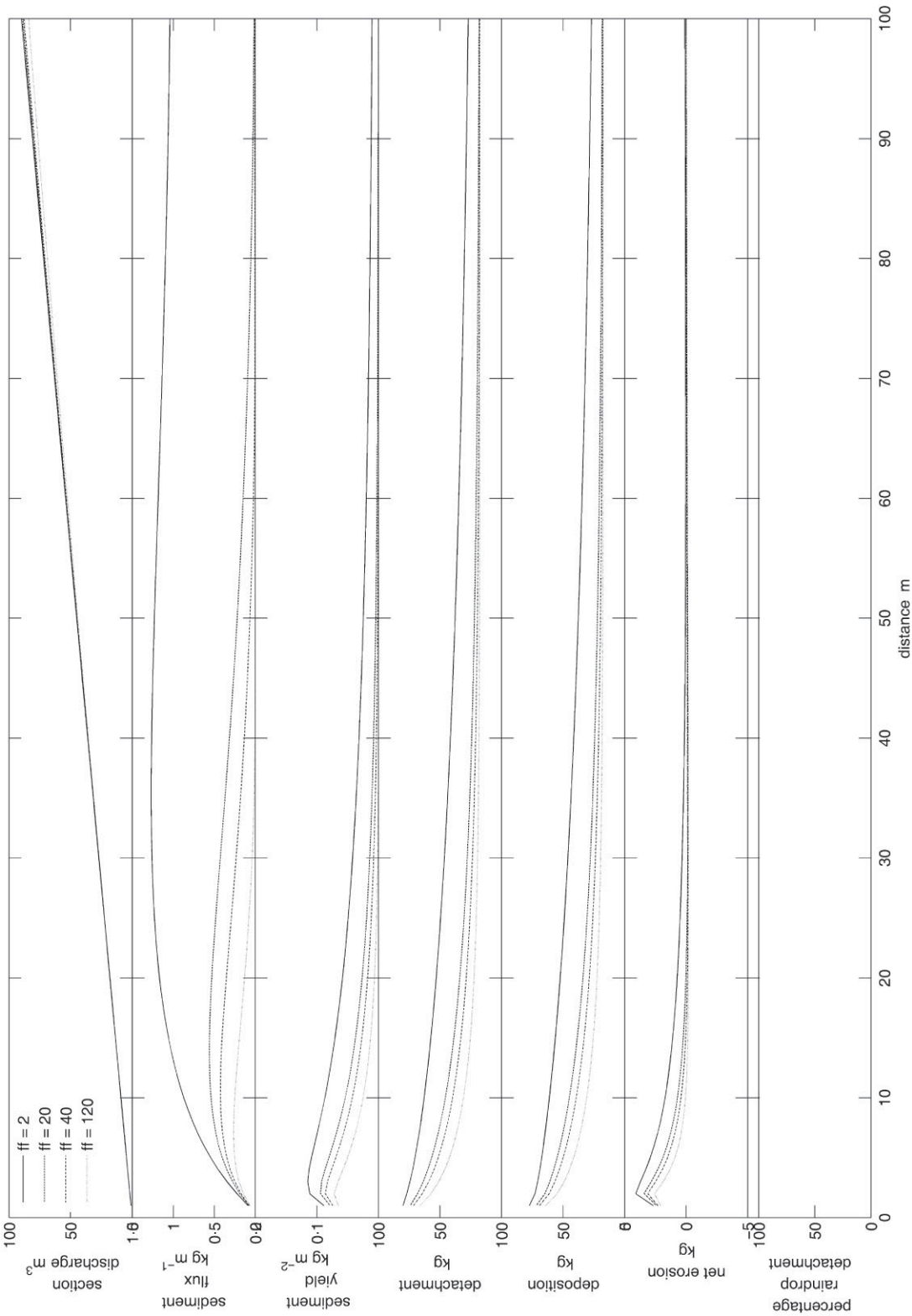

Figure A4. Sensitivity analysis on a uniform, planar 100 m long × 30 m wide slope according to friction factor considering unconcentrated erosion only.

DOI: 10.1002/esp

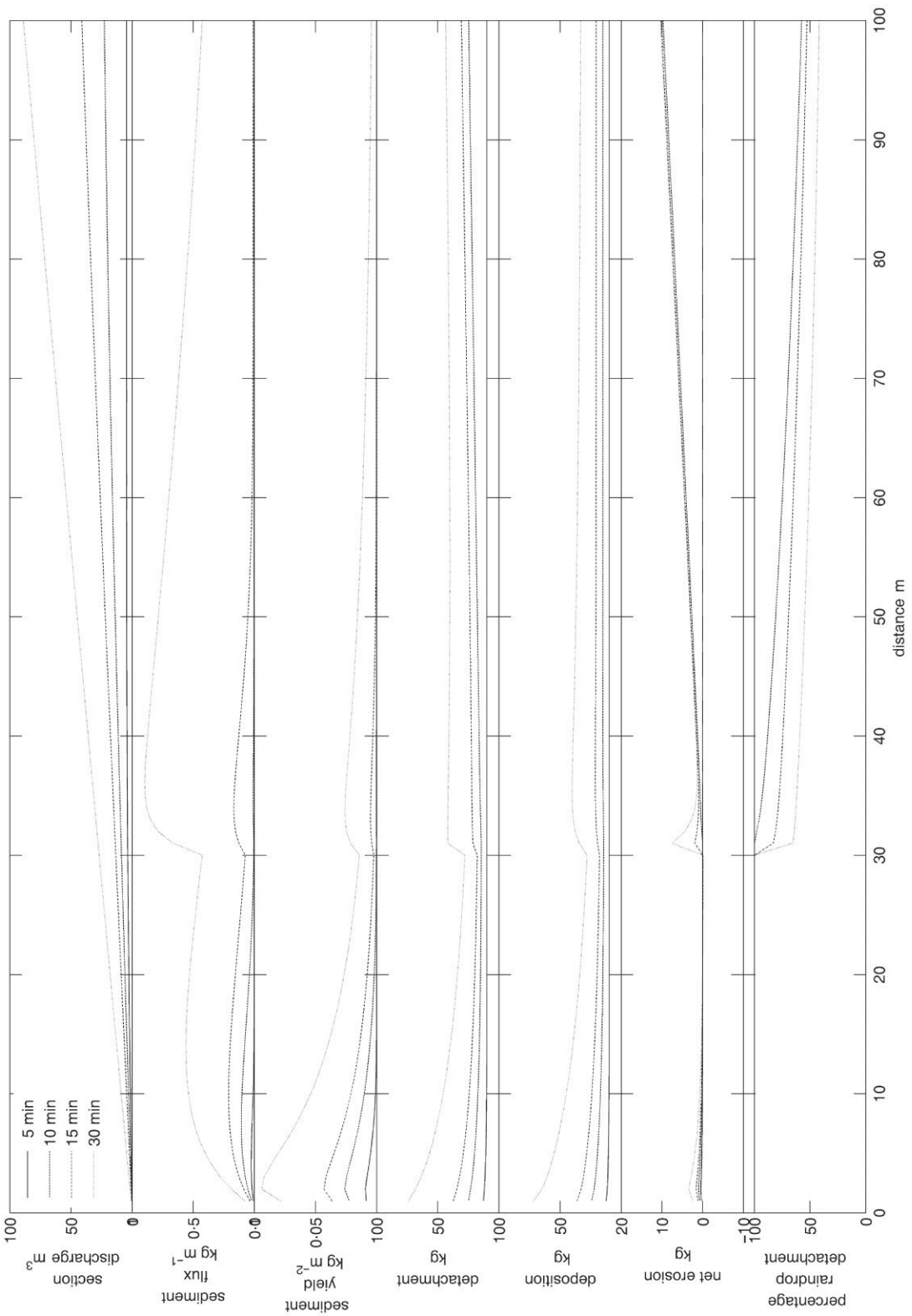

Figure A5. Sensitivity analysis on a uniform, planar 100 m long × 30 m wide slope according to rainfall duration considering both unconcentrated and concentrated erosion.

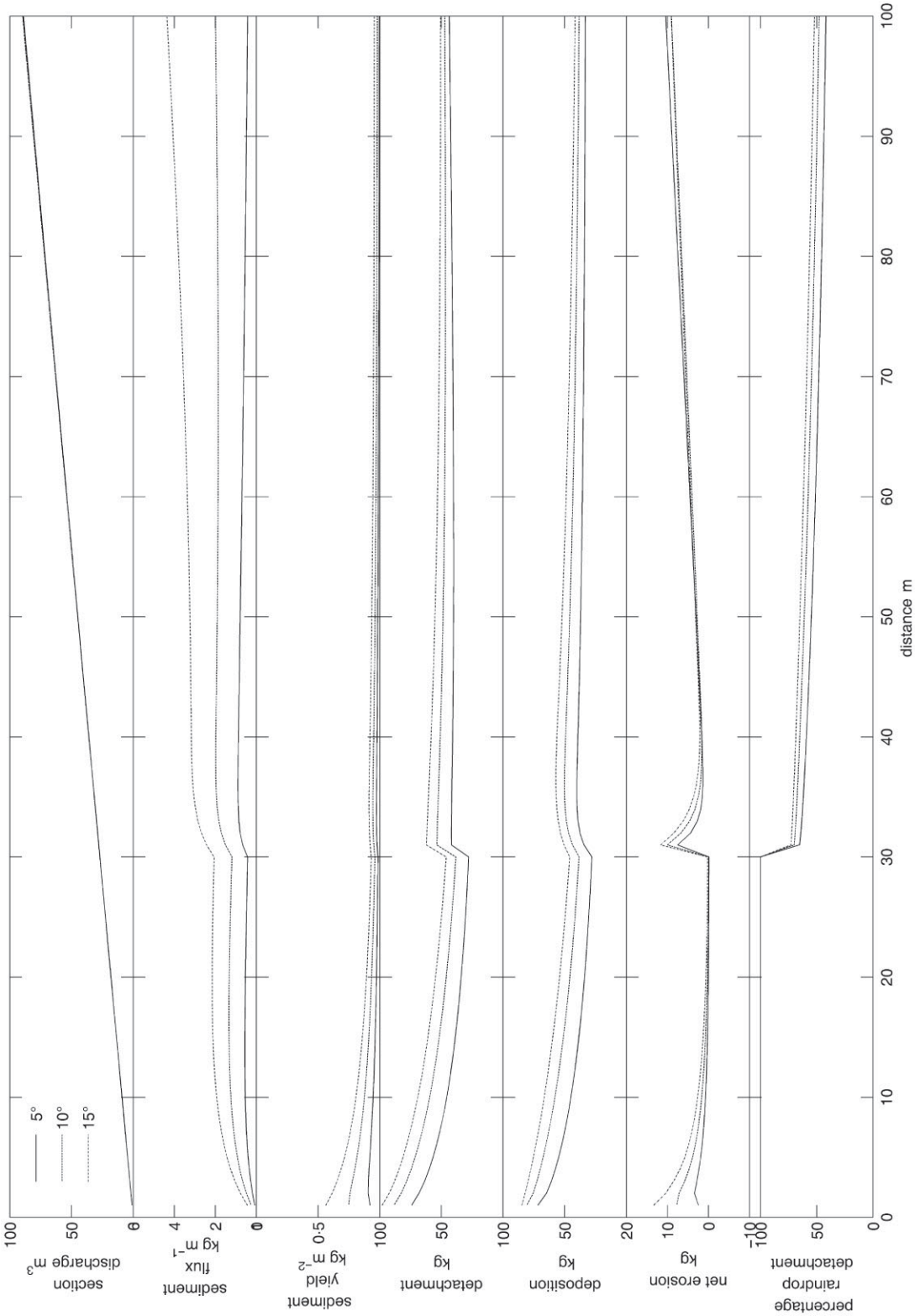

Figure A6. Sensitivity analysis on a uniform, planar 100 m long × 30 m wide slope according to slope angle considering both unconcentrated and concentrated erosion.

DOI: 10.1002/esp

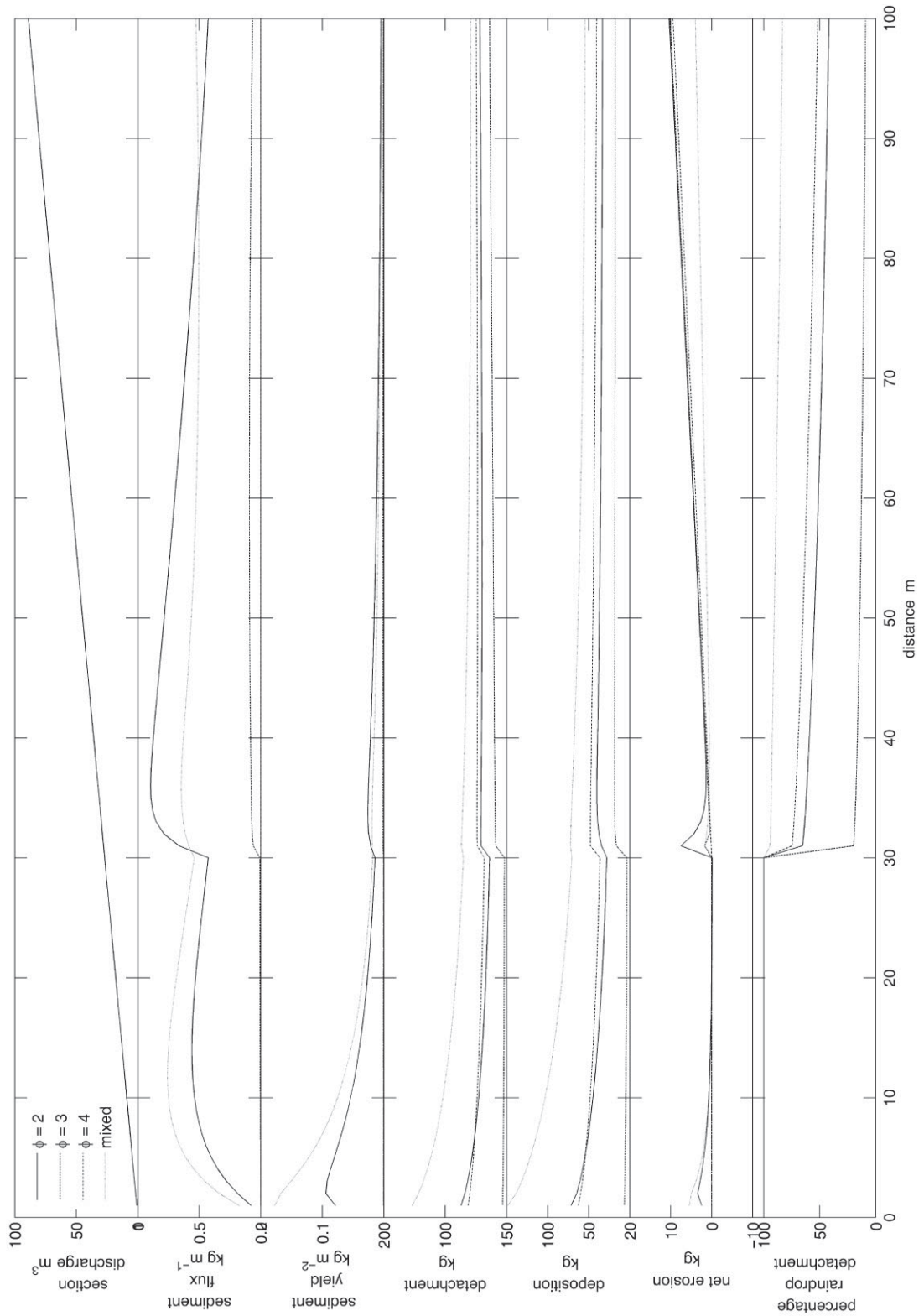

Figure A7. Sensitivity analysis on a uniform, planar 100 m long × 30 m wide slope according to grain size considering both unconcentrated and concentrated erosion.

DOI: 10.1002/esp

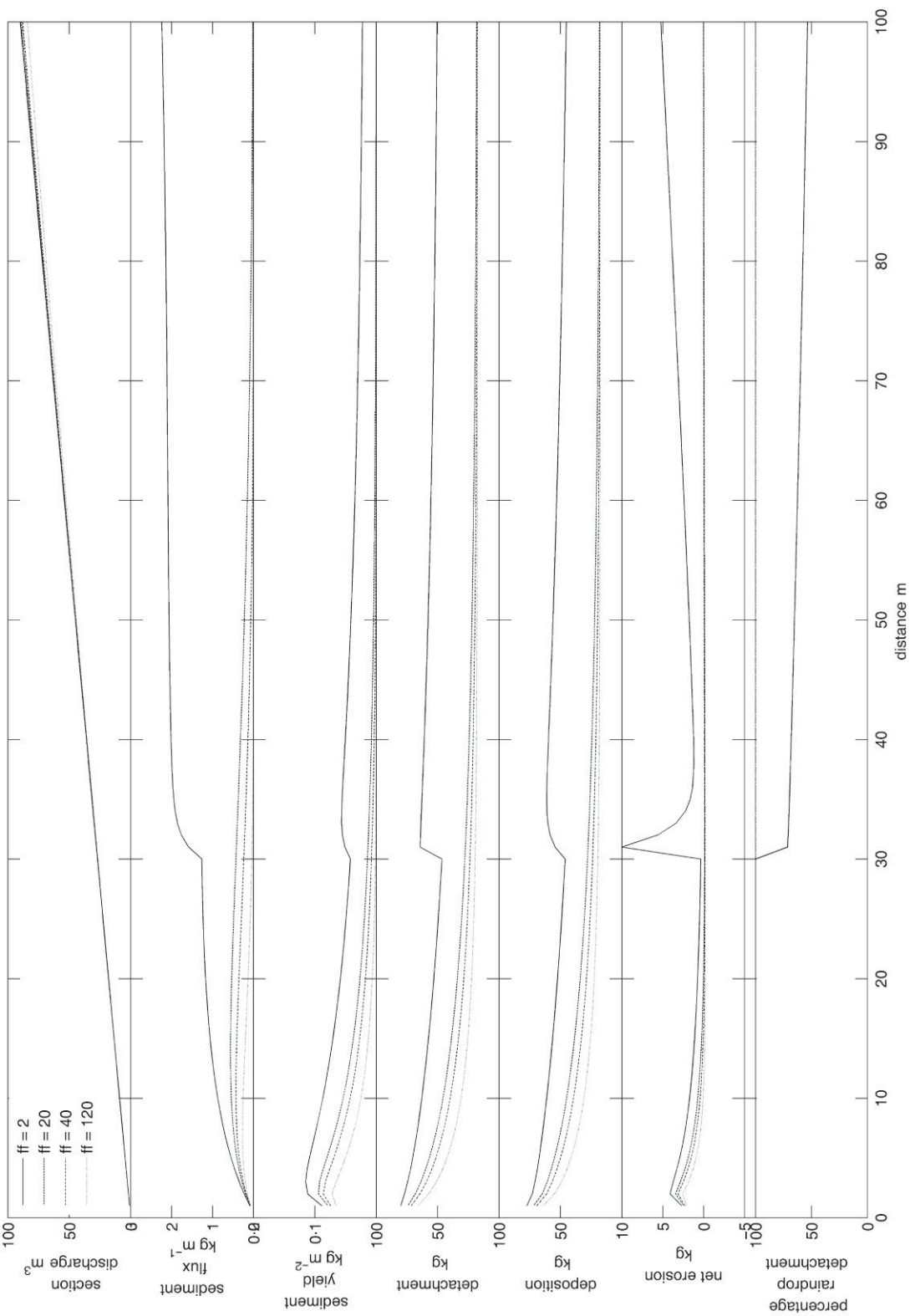

Figure A8. Sensitivity analysis on a uniform, planar 100 m long × 30 m wide slope according to friction factor considering both unconcentrated and concentrated erosion.

DOI: 10.1002/esp